**NEURO**

# Radiomics from magnetic resonance imaging may be used to predict the progression of white matter hyperintensities and identify associated risk factors

Zhenyu Shu[1] · Yuyun Xu[1] · Yuan Shao[1] · Peipei Pang[2] · Xiangyang Gong[1,3]

## Abstract

**Objective** The progression of white matter hyperintensities (WMH) varies considerably in adults. In this study, we aimed to predict the progression and related risk factors of WMH based on the radiomics of whole-brain white matter (WBWM).

**Methods** A retrospective analysis was conducted on 141 patients with WMH who underwent two consecutive brain magnetic resonance (MR) imaging sessions from March 2014 to May 2018. The WBWM was segmented to extract and score the radiomics features at baseline. Follow-up images were evaluated using the modified Fazekas scale, with progression indicated by scores $\geq 1$. Patients were divided into progressive ($n = 65$) and non-progressive ($n = 76$) groups. The progressive group was subdivided into any WMH (AWMH), periventricular WMH (PWMH), and deep WMH (DWMH). Independent risk factors were identified using logistic regression.

**Results** The area under the curve (AUC) values for the radiomics signatures of the training sets were 0.758, 0.749, and 0.775 for AWMH, PWMH, and DWMH, respectively. The AUC values of the validation set were 0.714, 0.697, and 0.717, respectively. Age and hyperlipidemia were independent predictors of progression for AWMH. Age and body mass index (BMI) were independent predictors of progression for DWMH, while hyperlipidemia was an independent predictor of progression for PWMH. After combining clinical factors and radiomics signatures, the AUC values were 0.848, 0.863, and 0.861, respectively, for the training set, and 0.824, 0.818, and 0.833, respectively, for the validation set.

**Conclusions** MRI-based radiomics of WBWM, along with specific risk factors, may allow physicians to predict the progression of WMH.

**Key Points**
• *Radiomics features detected by magnetic resonance imaging may be used to predict the progression of white matter hyperintensities.*
• *Radiomics may be used to identify risk factors associated with the progression of white matter hyperintensities.*
• *Radiomics may serve as non-invasive biomarkers to monitor white matter status.*

**Keywords** White matter · Magnetic resonance imaging · Risk factors · Retrospective studies · Neuroimaging

✉ Yuyun Xu
xuyuyun@hmc.edu.cn

✉ Xiangyang Gong
cjr.gxy@hotmail.com

1 Department of Radiology, Zhejiang Provincial People's Hospital, People's Hospital of Hangzhou Medical College, Hangzhou, China

2 GE Healthcare (China), Shanghai, China

3 Institute of Artificial Intelligence and Remote Imaging, Hangzhou Medical College, Hangzhou, China

## Abbreviations

| | |
|---|---|
| AUC | Area under the curve |
| AWMH | Progression of WMH in any (periventricular and/or deep) region |
| BMI | Body mass index |
| DTI | Diffusion tensor imaging |
| DWMH | Deep white matter hyperintensities |
| FLAIR | Fluid attenuated inversion recovery |
| GLCM | Gray-level co-occurrence matrix |
| ICC | Intraclass correlation coefficient |
| LASSO | The least absolute shrinkage and selection operator |
| LDL | Low-density lipoprotein |
| MRI | Magnetic resonance imaging |
| NAWM | Normal-appearing white matter |
| PWMH | Periventricular white matter hyperintensities |
| RLM | Run-length matrix |
| ROC | Receiver operating characteristic |
| ROI | Region of interest |
| WBWM | Whole-brain white matter |
| WMH | White matter hyperintensities |

## Introduction

White matter hyperintensities (WMH) refer to the neuroimaging feature of small blood vessel disease found during brain magnetic resonance imaging (MRI). WMH have been associated with cognitive decline, depression, and Alzheimer's disease [1]. Accordingly, it is particularly important to identify and prevent the progression of WMH [2]. However, this has been difficult as the pathogenesis of WMH remains unclear [3–5]. Certain factors such as age and hypertension have been associated with WMH [6], but the determinants involved in the formation of WMH are likely different from those involved in the progression of WMH [7]. Once the risk factors associated with the progression of WMH have been identified, early intervention strategies may be developed to attenuate brain injury.

Radiomics, which is a promising and rapidly growing discipline, is a method for extracting a large number of quantitative features from medical images and converting the information into mineable data [8–10]. These data can be subsequently analyzed to construct biomarkers for disease prediction and diagnosis through feature selection. Radiomics has been widely used in neurological diseases, including small vascular disease [4], multiple sclerosis [11], and traumatic brain injury [12]. Diffusion tensor imaging (DTI) or arterial spin labeling can detect microscopic changes in the whole-brain white matter (WBWM) to assess the severity and progression of WMH status, and some studies have revealed that microstructures have changed in normal-appearing white matter (NAWM) [13, 14]. NAWM is visually similar to healthy

tissues, yet WMH may be detected by advanced MRI techniques. Understanding the conversion of NAWM to WMH may further help identify patients at risk of developing progressive WMH, bringing valuable information for clinicians to offer precise preventive and therapeutic options to patients. Compared with those advanced MRI studies, radiomics has the benefit of using clinical routine MRI sequences to evaluate the status of WMH.

In our previous study using MRI [15], we found that the radiomics analysis of WMH penumbra was predictive of the development of WMH while in the early form of NAWM. However, this is difficult to achieve in the traditional clinic as WMH penumbra must be drawn manually and accurately, which is difficult and time-consuming. The WBWM, including normal white matter, WMH, and the penumbra, can easily be extracted on T1-weighted fluid-attenuated inversion recovery (FLAIR) using the software. Accordingly, we utilized the radiomics score of WBWM from conventional brain MRI scans to predict the progression and identify associated risk factors of WMH. The purpose of the current study was to investigate whether radiomics of WBWM could be used to predict the progression and identify associated risk factors of WMH based on radiomics features extracted from different brain regions.

## Materials and methods

This retrospective study was approved by our institutional review board, and the requirement for informed consent was waived.

### Study population

The MRI data of 1073 patients who underwent brain MRI scans at our hospital from March 2014 to May 2018 were retrospectively analyzed. Among the patients, 141 patients with WMH who underwent two consecutive brain MRI scans were used in this study, including 71 males and 70 females (mean age, 67 years; range, 50–87 years). Patients were included based on the following criteria: (1) WMHs were visible on T2-weighted imaging and T2FLAIR; (2) patients were ≥ 50 years of age; (3) no stroke lesions on current diffusion-weighted imaging (except lacunar infarction); and (4) no indications of multiple sclerosis, Alzheimer's disease, Parkinson's disease, or traumatic brain injury. The exclusion criteria were as follows: (1) non-vascular white matter lesions (i.e., demyelinating autoimmune disease, metabolism, poison, infection); (2) signs of intracranial hemorrhage; or (3) serious head motion artifacts.

Clinicodemographic data were collected, including age, gender, diabetes status, hypertension, hyperlipidemia, and coronary heart disease. Smoke and alcohol consumption history

in the past 5 years was also obtained. Smoking was defined as having more than 10 cigarettes per day, and alcohol consumption was defined as the amount of ethanol $\geq 40$ g per day for men and $\geq 20$ g per day for women, respectively. Hypertension was defined as a systolic blood pressure of $\geq 140$ mmHg, diastolic pressure of $\geq 90$ mmHg, or with the current usage of antihypertensive medications. Hyperlipidemia was defined as the overnight fasting low-density lipoprotein (LDL) of $\geq 130$ mg/dl.

## MRI acquisition

All brain MRI scans were performed in a local hospital on a 3.0 T MRI scanner (Discovery MR 750, GE Healthcare) with an eight-channel head coil using the same MR parameters. The routine sequences included T1FLAIR, T2-weighted imaging, diffusion-weighted imaging, and T2FLAIR. Axial T2FLAIR was used for observing the WMH with the following parameters: repetition time/echo time = 9000/120 ms and field of view = $256 \times 256$ mm, matrix = $256 \times 256$, flip angle = 160°, echo chain = 18, bandwidth = 50, section thickness = 5 mm, inter-slice gap = 0. T1FLAIR was used to segment the white matter with repetition time = 1750 ms, echo time = 24 ms, field of view = $256 \times 256$ mm, resolution = $256 \times 256$, flip angle = 111°, echo chain = 10, bandwidth = 31.25, section thickness = 5 mm, and inter-slice gap = 0.

## Processing of MRI scans

All T1FLAIR baseline images were imported into the SPM12 software (https://www.fil.ion.ucl.ac.uk/spm/software/spm12/) for automatic segmentation of the white matter. The WBWM was manually modified by an experienced neuroradiologist who was blinded to the clinical data using the ITK-SNAP software (http://www.itksnap.org/pmwiki/pmwiki.php). This was accomplished by the following steps: (1) removal of non-brain tissues, brainstem, and cerebellum; and (2) modified white matter segmentation. The WBWM is shown in Figure S1.

The segmented WBWM was imported into the AK software (Artificial Intelligence Kit V3.0.0.R, GE Healthcare) for feature extraction. Radiomics features, including histogram, formfactor, gray-level co-occurrence matrix (GLCM), and run-length matrix (RLM), were calculated. Several pre-processing steps using the AK software were performed to extract the radiomics features. First, all WBWM images were resampled to change the voxels to $1 \times 1 \times 1$ mm by linear interpolation to eliminate the effect of anisotropy on the features. Gaussian filtering was used to reduce noises in the image. The magnetic field migration correction was performed, which also assisted in reducing external interference factors. Finally, histogram mapping and intensity standardization were

performed to limit the gray level of all images to 0–255 for comparative analysis of the features.

## Progression of WMH

The visual rating scale proposed by Prins et al [16] was used to assess the progression of WMH in follow-up MRI scans, ranging from − 3 to + 3 in periventricular regions and − 4 to + 4 in deep regions. The progression of WMH was defined as a score of $\geq 1$. Two experienced neuroradiologists, who were blinded to clinical information, reviewed the images independently to assess the changes in WMH. A disagreement between the neuroradiologists was resolved by discussion until a consensus was reached. Since the pathogenesis of periventricular WMH and subcortical WMH may be different [17], the group showing progressive WMH was divided into three subsets based on regions: periventricular white matter hyperintensity (PWMH) progression, deep white matter hyperintensity (DWMH) progression, and progression of WMH in any periventricular or deep region (AWMH). PWMH was defined as WMH directly connected to ventricles, while DWMH was defined as WMH connected to the subcortical area without extending to ventricles [18, 19].

## Extraction of radiomics features and construction of the radiomics signature

Patients in each subgroup were randomly divided into the training ($n = 98$) and validation ($n = 43$) sets according to a ratio of 7 to 3, respectively, and the radiomics features were extracted for each patient. In total, 328 features were extracted for each patient, including 32 histogram features, eight formfactor features, 144 GLCM features, and 144 RLM features. The extracted features were standardized, and dimension reductions were performed. The least absolute shrinkage and selection operator (LASSO) was used to select the most powerful features of the training set to build the radiomics signature. Next, the radiomics signature was used to calculate the radiomics score (rad-score) for each patient, and this score was defined as the risk score for the progression of WMH. A radiomics score was calculated for each patient in the validation set using the same formula constructed for the training set. The predictive accuracy of the radiomics signature was quantified by the area under the receiver operating characteristic (ROC) curve (AUC) in the training and validation sets. Additional information about the process of radiomics feature extraction and feature selection can be found in the Supplementary Materials.

We initially chose 30 random images for the region of interest (ROI) segmentation and feature extraction, which was performed independently by the two neuroradiologists (combined 19 years of experience) who were blinded to the clinical information. The inter-observer reproducibility of

feature extraction was initially analyzed between the two radiologists. For assessing intra-observer reproducibility, the first neuroradiologist repeated the feature extraction process twice during a 2-week period using the same procedures.

## Construction and assessment of the radiomics model

The clinical data of patients with progressive WMH in each subgroup were dichotomized, and the differences in the radiomics score between the two classifications were compared for selecting potential predictive variables. In the training set, a univariate logistic regression analysis was performed for each potential predictive factor. Next, a multivariable logistic regression analysis was used to establish a radiomics model for assessing the progression of WMH, combining the independent clinical risk factors and radiomics signature. Internal validation of the radiomics model was performed with the validation set. The model was assessed using a calibration curve, and the Hosmer-Lemeshow test was performed to assess the goodness-of-fit of the model. Furthermore, the AUC was used to evaluate the discrimination of the model.

## Statistical analysis

The statistical analyses were performed using SPSS 17.0, MedCalc15.8 software, and GraphPad Prism 6. The Kolmogorov-Smirnov test was applied to evaluate the normality of distribution, and the chi-square test was used for categorical data. This study carried out two classifications of continuous variables, including body mass index (BMI) with $\geq 25$ kg/m$^2$ being defined as obese, age with $\geq 60$ years being

defined as an older adult, and low-density lipoprotein (LDL) levels with $\geq 130$ mg/dl being defined as hyperlipidemia. After conducting a comparative analysis of radiomics scores between the two subgroups for each risk factor, through the Student's $t$ test or Mann-Whitney test, statistically significant risk factors were included in the univariate logistic regression to evaluate whether the risk factor was independently associated with the progression of WMH. A predictive model was established using the multivariable logistic stepwise regression for progression of WMH in sub-regions, and the predictive performance was evaluated with the ROC curve. Finally, a correlation analysis was performed between the independent risk factors and radiomics signatures. Statistically significant values were those with $p$ values of $\leq 0.05$.

## Results

### Patient characteristics

The radiomics workflow is presented in Fig. 1. A total of 141 patients with WMH were included in the study, of which 65 subjects were divided into the progression group and 76 subjects in the non-progression group. The number of patients having coronary heart disease or hyperlipidemia reached statistically significant levels between the two groups ($p \leq 0.05$). No significant differences were observed in the other clinical factors, including MR interval, age, BMI, diabetes, hypertension, smoking history, alcoholic history, and baseline Fazekas scores (all $p \leq 0.05$), as shown in Table 1.
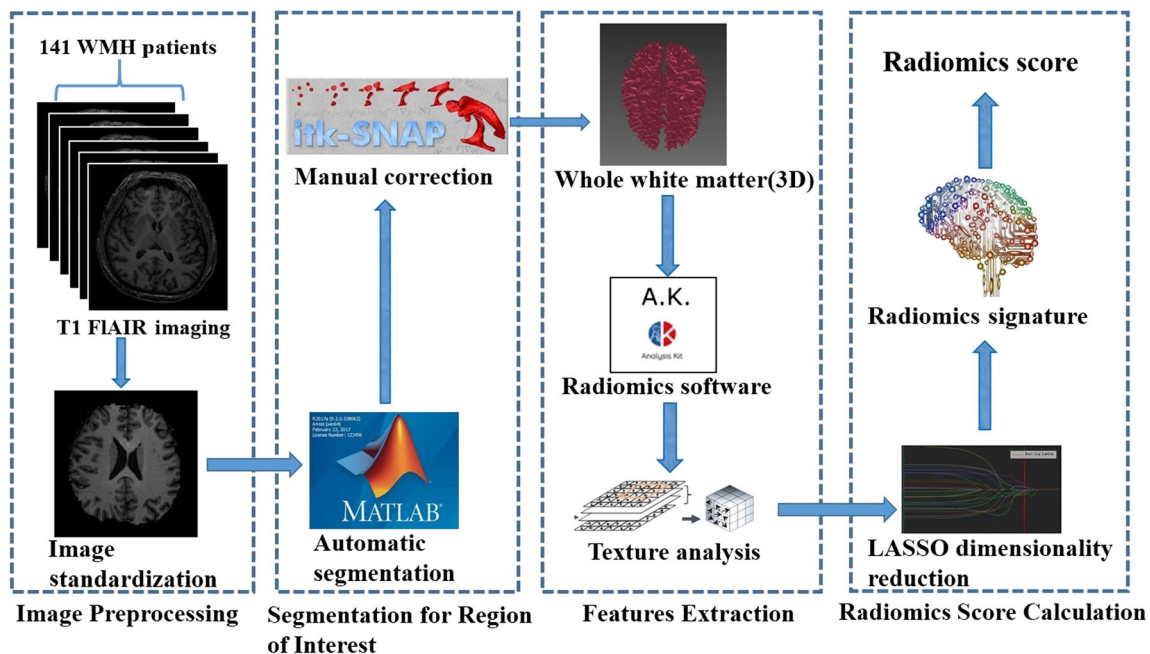


Fig. 1 Radiomics workflow of normal white matter

**Table 1** Clinical and demographic information of patients in this study

| Characteristic | Study Population ($n = 141$) | Progression of WMH | | $p$ value |
|---|---|---|---|---|
| | | No ($n = 76$) | Yes ($n = 65$) | |
| **Demographics** | | | | |
| Age (y)* | 66.8 ± 8.2 | 64.3 ± 7.1 | 67.9 ± 8.3 | 0.372 |
| Male sex (n)▲ | 71 (50.4) | 35 (46.1) | 36 (55.4) | 0.269 |
| MR interval (months)* | 38 ± 4 | 37 ± 3 | 38 ± 4 | 0.089 |
| **Cardiovascular risk factors** | | | | |
| BMI (kg/m²)* | 23.65 ± 2.93 | 23.53 ± 2.92 | 23.79 ± 2.96 | 0.599 |
| Hypertension (n)▲ | 87 (61.7) | 43 (56.6) | 44 (67.7) | 0.176 |
| Diabetes mellitus (n)▲ | 49 (34.8) | 24 (31.6) | 25 (38.5) | 0.392 |
| Coronary heart disease (n)▲ | 23 (16.3) | 7 (9.2) | 16 (24.6) | 0.014 |
| Hyperlipidemia (n)▲ | 54 (38.3) | 16 (21.1) | 38 (58.5) | < 0.05 |
| Smoking in past 5 years (n)▲ | 20 (14.2) | 8 (10.5) | 12 (18.5) | 0.178 |
| Alcohol intake in past 5 years (n)▲ | 16 (11.3) | 12 (15.8) | 4 (6.2) | 0.072 |
| **The Fazekas score of WMH at baseline** | | | | |
| 0 (n) | 0 | 0 | 0 | |
| 1 (n) | 11 (7.8) | 7 (9.2) | 4 (6.2) | 0.5 |
| 2 (n) | 38 (26.95) | 23 (30.2) | 15 (23.1) | 0.338 |
| 3 (n) | 31 (21.99) | 18 (23.7) | 13 (20) | 0.599 |
| 4 (n) | 24 (17.02) | 13 (17.1) | 11 (16.9) | 0.977 |
| 5 (n) | 27 (19.15) | 11 (14.5) | 16 (24.6) | 0.127 |
| 6 (n) | 10 (7.09) | 4 (5.3) | 6 (9.2) | 0.36 |

Data represents the mean ± SD, number of participants (%). Comparisons between non-progression group and progression group. * Data are mean ± standard deviation. ▲ Data are the number of patients, with percentages in parentheses. *MR*, magnetic resonance; *BMI*, body mass index; *WMH*, white matter hyperintensities

## Inter-observer and intra-observer reproducibility of radiomics feature extraction

The intra-observer intra-class correlation coefficient (ICC), which was calculated based on two measurements from the first neuroradiologist, ranged from 0.826 to 0.937. The inter-observer agreement between the two neuroradiologist readers ranged from 0.773 to 0.916. These results indicated favorable intra- and inter-observer reproducibility of the feature extraction process.

## Radiomics signatures

The most powerful characteristics were selected to construct the radiomics signatures, which included eight features in the AWMH subgroup, nine features in the PWMH subgroup, and 11 features in the DWMH subgroup. Additional information about these features is shown in Table S1. The radiomics properties extracted from the three subgroups were used to develop the radiomics signatures by LASSO. Additional details regarding the creation of the radiomics and the results may be found in the Supplementary Materials. Using the formula for the radiomics signature, the rad-score was calculated and found to be significantly different between progression and non-

progression groups in the AWMH, PWMH, and DWMH subgroups (all $p \leq 0.05$). The predictive efficacies for the radiomics scores of the training and validation sets were also significantly different between the three subgroups. The AUC values were 0.758 and 0.714 for AWMH, 0.749 and 0.697 for PWMH, and 0.775 and 0.717 for DWMH (Table 2).

## Clinical factors in the progressive WMH subgroups

Among all of the clinical risk factors in subgroups, age, sex, hypertension, smoking, and hyperlipidemia were associated with AWMH progression of ($p < 0.05$); age, sex, hypertension, coronary heart disease, smoking, and hyperlipidemia were associated with PWMH progression ($p < 0.05$); age, weight, smoking, and hyperlipidemia were associated with the progression of DWMH ($p < 0.05$); see Table 3 for more details.

## Logistic regression analyses of progression in three WMH subgroups

Multivariable logistic regression analyses revealed specific radiomics signatures that were independent predictors for all of the subgroups. Age and hyperlipidemia were independent predictors of progression of AWMH, age

**Table 2** Comparison of radiomic scores between the training and validation sets in the three subgroups of AWMH, PWMH, and DWMH

| Group | AWMH | | PWMH | | DWMH | |
|---|---|---|---|---|---|---|
| | Training set (n = 98) | validation set (n = 43) | Training set (n = 98) | validation set (n = 43) | Training set (n = 98) | validation set (n = 43) |
| Non− progression | 0.67 ± 1.282 | 0.615 ± 1.261 | 0.413 ± 1.211 | 0.635 ± 1.211 | 0.660 ± 1.23 | 0.579 ± 1.166 |
| Progression | − 0.605 ± 1.375 | − 0.423 ± 1.514 | − 0.621 ± 1.109 | − 0.373 ± 1.337 | − 0.525 ± 1.203 | − 0.684 ± 1.413 |
| p value | < 0.001 | < 0.001 | < 0.001 | < 0.001 | < 0.001 | < 0.001 |
| AUC | 0.758 | 0.714 | 0.749 | 0.697 | 0.775 | 0.717 |
| Sensitivity | 0.815 | 0.646 | 0.892 | 0.625 | 0.823 | 0.629 |
| Specificity | 0.717 | 0.896 | 0.523 | 0.767 | 0.719 | 0.753 |
| Accuracy | 0.794 | 0.725 | 0.766 | 0.721 | 0.783 | 0.734 |
| F1 Score | 0.741 | 0.722 | 0.673 | 0.614 | 0.726 | 0.713 |

*AWMH*, white matter hyperintensities in any (periventricular and/or deep) region; *PWMH*, periventricular white matter hyperintensities; *DWMH*, deep white matter hyperintensities; *AUC*, area under the curve

**Table 3** Statistical analysis of the radiomics scores based on the subgroups of clinical risk factors

| | | Progression of AWMH (n = 65) | Progression of PWMH (n = 44) | Progression of DWMH (n = 53) |
|---|---|---|---|---|
| Age | ≤ 60 | − 0.566 ± 1.62 | − 0.594 ± 1.664 | − 0.537 ± 1.079 |
| | > 60 | − 0.465 ± 1.295 | − 0.486 ± 1.578 | − 0.436 ± 1.63 |
| | p value | 0.003* | 0.032* | 0.001* |
| Gender | Male | − 0.392 ± 1.314 | − 0.252 ± 1.345 | − 0.504 ± 1.268 |
| | Female | − 0.694 ± 1.613 | − 0.829 ± 0.947 | − 0.616 ± 1.005 |
| | p value | 0.014* | 0.038* | 0.324 |
| BMI | < 25 | − 0.268 ± 1.539 | − 0.474 ± 1.307 | − 0.431 ± 1.347 |
| | ≥ 25 | − 0.528 ± 1.407 | − 0.545 ± 0.953 | − 0.707 ± 1.006 |
| | p value | 0.515 | 0.224 | 0.015* |
| Diabetes mellitus | No | − 0.343 ± 1.478 | − 0.451 ± 1.372 | − 0.391 ± 1.391 |
| | Yes | − 0.619 ± 1.482 | − 0.627 ± 1.671 | − 0.502 ± 1.507 |
| | p value | 0.433 | 0.683 | 0.284 |
| Hypertension | No | − 0.062 ± 1.576 | − 0.21 ± 1.589 | − 0.223 ± 1.5 |
| | Yes | − 0.482 ± 1.815 | − 0.83 ± 1.685 | − 0.248 ± 1.55 |
| | p value | 0.006* | 0.016* | 0.463 |
| Coronary heart disease | No | − 0.312 ± 1.748 | − 0.314 ± 1.145 | − 0.529 ± 1.164 |
| | Yes | − 0.872 ± 1.447 | − 1.325 ± 0.664 | − 0.886 ± 1.267 |
| | p value | 0.188 | 0.001* | 0.379 |
| Alcohol intake | No | − 0.324 ± 1.486 | − 0.334 ± 1.574 | − 0.332 ± 1.41 |
| | Yes | − 0.613 ± 1.704 | − 0.709 ± 1.627 | − 0.632 ± 1.458 |
| | p value | 0.184 | 0.732 | 0.286 |
| Smoking | No | − 0.287 ± 1.653 | − 0.444 ± 1.645 | − 0.292 ± 1.436 |
| | Yes | 0.056 ± 1.795 | − 0.03 ± 1.664 | 0.061 ± 1.866 |
| | p value | 0.003* | 0.017* | 0.021* |
| Hyperlipidemia | No | − 0.185 ± 1.576 | − 0.262 ± 1.549 | − 0.111 ± 1.436 |
| | Yes | − 0.818 ± 3.066 | − 0.937 ± 2.939 | − 1.253 ± 1.315 |
| | p value | 0.027* | 0.015* | 0.004* |

*p < 0.05; *BMI*, body mass index; *AWMH*, white matter hyperintensities in any (periventricular and/or deep) region; *PWMH*, periventricular white matter hyperintensities; *DWMH*, deep white matter hyperintensities

and BMI were independent predictors of DWMH, and hyperlipidemia was an independent predictor of PWMH. Prediction models were established based on the results of the multivariate logistic regression. The Hosmer-Lemeshow test in the three subgroups showed no significant differences in the goodness-of-fit for the training set models ($p = 3.493$, 2.385, and 2471 for AWMH, DWMH, and PWMH, respectively). The calibration curve showed excellent calibration in the training and validation sets of the three subgroups. Additionally, we evaluated the accuracy of the radiomics model for the training and validation sets in the three subgroups. For AWMH, the AUC was 0.848 and 0.824, for the training and validation sets, respectively. For PWMH, the AUC was 0.863 and 0.818, respectively. For DWMH, the AUC was 0.861 and 0.833, respectively (Table 4; Figs. 2, 3, and 4).

## Correlations between radiomics signatures and independent risk factors

Seven radiomics features were significantly correlated with independent risk factors (Figs. 5 and 6). In the AWMH subgroup, SurfaceArea of the formfactor feature was negatively correlated with age and LDL ($r = -0.571$, $-0.403$, $p < 0.001$), and InverseDifferenceMoment_ALLDirection_offset1_SD of GLCM feature was positively correlated with age ($r = 0.638$, $p < 0.001$). In the PWMH subgroup, Compactness2 of the formfactor feature was negatively correlated with LDL ($r = -0.592$, $p < 0.001$), and InverseDifferenceMoment_angle0_offset7 of GLCM feature was positively correlated with LDL ($r = 0.204$, $p < 0.001$). In the DWMH subgroup, LongRunEmphasis_angle135_offset7 of RLM feature was negatively correlated with age ($r = -0.293$, $p < 0.001$), and GLCMEntropy_angle45_offset4 of GLCM characteristic was positively correlated with age ($r = 0.301$, $p = 0.006$). Lastly, InverseDifferenceMoment_angle0_offset7 of the GLCM feature was positively correlated with BMI ($r = 0.394$, $p < 0.001$).

## Discussion

We used radiomics to predict the progression of WMH and identify the associated risk factors. Our findings suggest that

**Table 4** Risk factors associated with the progression of WMH in different regions by logistic regression analysis

| Subgroups | Univariate logistic regression | | Multivariate logistic regression | |
|---|---|---|---|---|
| | OR (95%CI) | *p* value | OR (95%CI) | *p* value |
| **AWMH group** | | | | |
| Age (years) (< 60 vs. ≥ 60) | 2.326 (1.036 − 5.226) | 0.041 | 4.264 (1.447 − 12.565) | 0.009 |
| Sex (male vs. female) | 0.963 (0.437 − 2.122) | 0.925 | NA | NA |
| Hypertension (No vs. Yes) | 1.356 (0.594 − 3.099) | 0.470 | NA | NA |
| Smoking (No vs. Yes) | 2.980 (0.851 − 10.429) | 0.088 | NA | NA |
| Hyperlipidemia (No vs. Yes) | 5.249 (2.208 − 12.479) | < 0.001 | 3.787 (1.407 − 10.191) | 0.008 |
| Radiomics score (per 0.1 increase) | 0.473 (0.333 − 0.673) | < 0.001 | 0.443 (0.292 − 0.672) | < 0.001 |
| **PWMH group** | | | | |
| Age (years) (< 60 vs. ≥ 60) | 2.895 (1.206 − 6.951) | 0.017 | NA | NA |
| Sex (male vs. female) | 0.983 (0.419 − 2.307) | 0.968 | NA | NA |
| Hypertension (No vs. Yes) | 1.383 (0.564 − 3.388) | 0.478 | NA | NA |
| Coronary heart disease (No vs. Yes) | 3.594 (1.125 − 11.484) | 0.071 | NA | NA |
| Smoking (No vs. Yes) | 1.867 (0.465 − 7.494) | 0.379 | NA | NA |
| Hyperlipidemia (No vs. Yes) | 7.944 (3.052 − 20.682) | < 0.001 | 5.495 (1.739 − 17.361) | 0.004 |
| Radiomics score (per 0.1 increase) | 0.380 (0.246 − 0.588) | < 0.001 | 0.336 (0.191 − 0.590) | < 0.001 |
| **DWMH group** | | | | |
| Age (years) (< 60 vs. ≥ 60) | 3.068 (1.309 − 7.191) | 0.01 | 4.576 (1.453 − 14.413) | 0.009 |
| Body Mass Index (kg/m²) (< 25 vs. ≥ 25) | 5.750 (2.346 − 14.094) | < 0.001 | 4.541 (1.585 − 13.006) | 0.005 |
| Smoking (No vs. Yes) | 3.257 (0.976 − 10.873) | 0.055 | NA | NA |
| Hyperlipidemia (No vs. Yes) | 1.019 (0.877 − 11.82) | 0.809 | NA | NA |
| Radiomics score (per 0.1 increase) | 0.423 (0.283 − 0.632) | < 0.001 | 0.375 (0.232 − 0.607) | < 0.001 |

*NA*, not available. These variables were evaluated in the multivariate logistic regression model, so the OR and *p* values were not available. *AWMH*, white matter hyperintensities in any (periventricular and/or deep) region; *PWMH*, periventricular white matter hyperintensities; *DWMH*, deep white matter hyperintensities
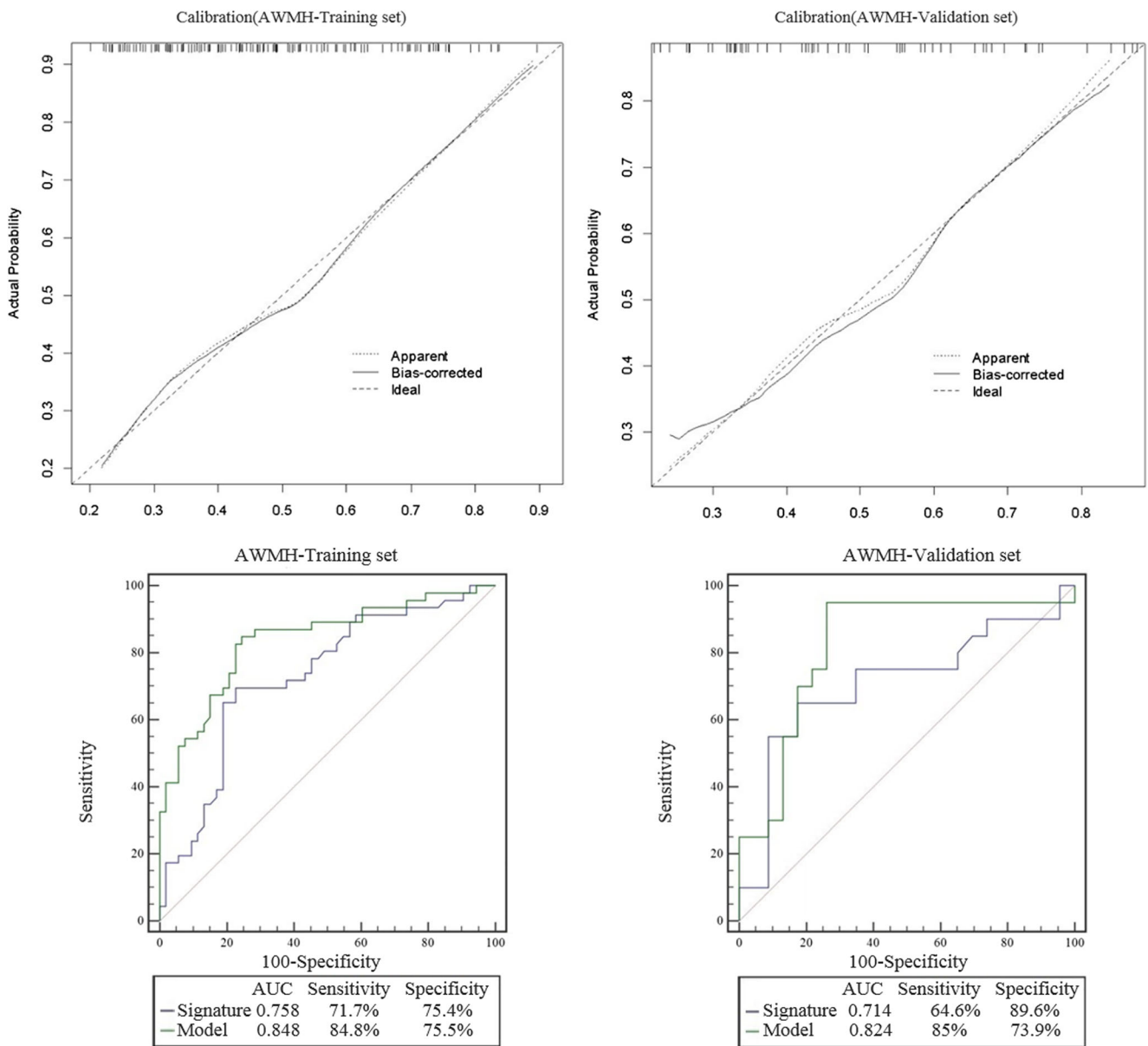
**Fig. 2** Calibration of the radiomics model for progression of WMH in any region of the training and validation sets. The dashed line represents a reference line where an ideal model would lie. The dotted line represents the performance of a hybrid model, while the solid line corrects for any bias in the hybrid model. The prediction performance of the ROC curves for AWMH and the AUC were 0.848 and 0.824, respectively

radiomics of WBWM could be used to predict the progression of WMH, which may support the theory of the existence of WBWH penumbra proposed by Maillard et al [2]. We also found that the clinical risk factors associated with the progression of WMH were different in PWMH and DWMH, suggesting that the pathogenesis may be different between these regions [20, 21]. Finally, specific radiomics signatures were found to be associated with risk factors for the progression of WMH, revealing the potential pathophysiological transformations from NAWM to WMH.

One of the advantages of the current study is that we extracted radiomics features from WBWM other than sporadic and progressive WMH, which could reflect the changes in white matter structures from NAWM to WMH, suggesting that it may be more powerful than features from WMH alone. The microstructural integrity of NAWM changed due to axonal injury and demyelination [22], and we believe this may be the reason for the significant differences in radiomics scores detected between the progression and non-progression groups. In addition, the radiomics score of the DWMH subgroup was lower than that of PWMH, which indicated that the heterogeneity of PWMH was more remarkable. This finding is consistent with a previous pathological finding that progression between DWMH and PWMH is different [23], yet it supports our hypothesis that radiomics may reflect the pathophysiological changes of WMH.
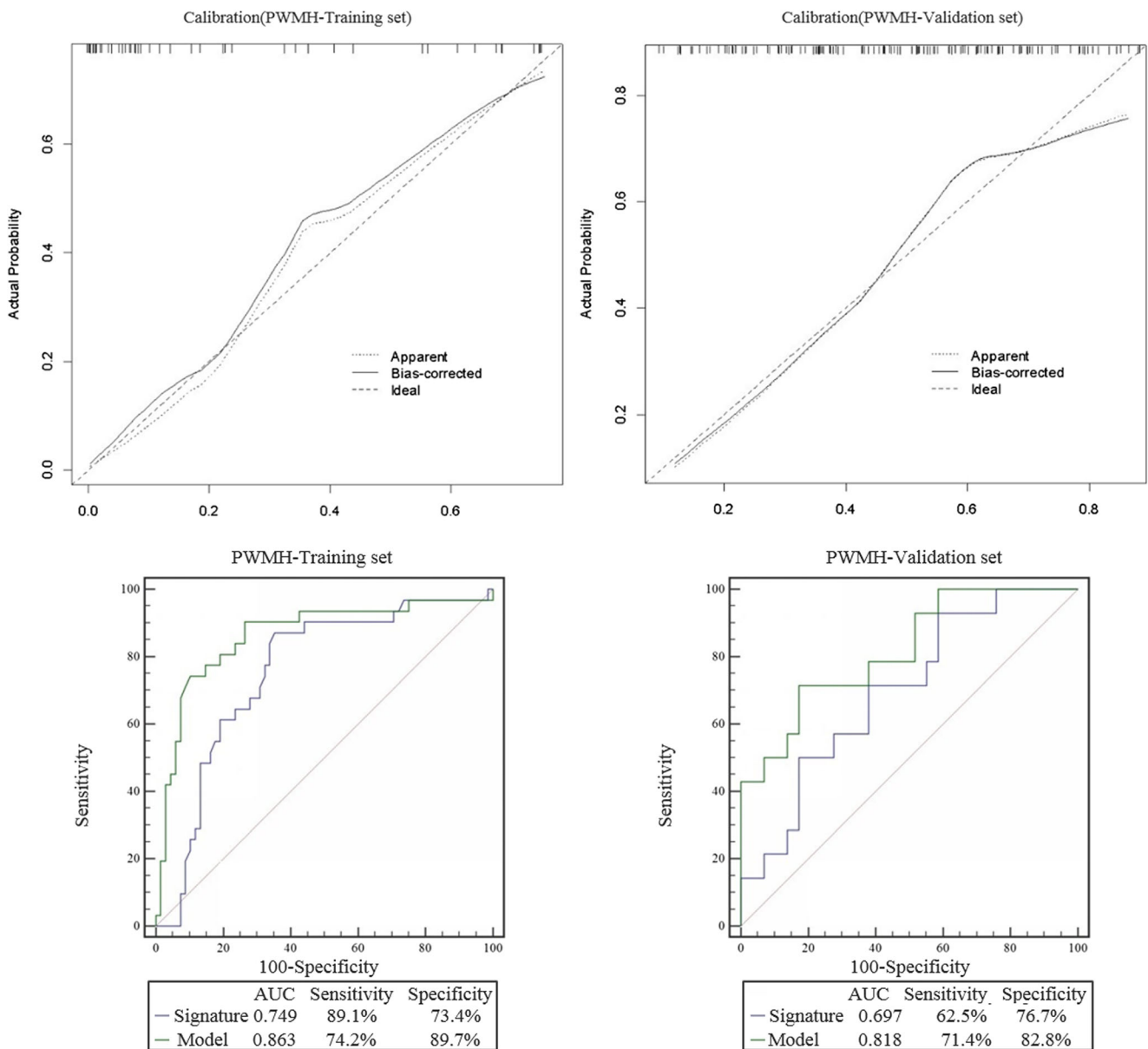
**Fig. 3** Calibration of the radiomics model for progression of periventricular WMH in the training and validation sets. The dashed line represents a reference line where an ideal model would lie. The dotted line represents the performance of a hybrid model, while the solid line corrects for any bias in the hybrid model. The prediction performance of the ROC curves for AWMH and the AUC were 0.863 and 0.818, respectively

Furthermore, we demonstrated that the clinical factors pertinent to the progression of WMH were selectively associated with radiomics signatures in different regions. Accordingly, the combination of the prediction model and risk factors was more effective than radiomics alone, implying that specific risk factors may accelerate the progression of WMH. In fact, microvascular structures are changed in MRI scans of visually NAWM [24–26]. Previously, Maillard et al [27] suggested that the early detection of microstructural damage in NAWM would require advanced MRI techniques, such as diffusion tensor imaging (DTI), rather than conventional MRI

sequences like T1FLAIR to quantify the NAWM integrity. However, our findings suggest that conventional sequences, such as T1FLAIR, when combined with radiomics can be used to quantify heterogeneity of visually NAWM.

We noticed that some risk factors, such as high blood pressure, did not survive in our regression model, though hypertension is thought to be a major burden of WMH. We suspect that patients with hypertension in this study were taking antihypertensive drugs for a long time, which might lead to changes in NAWM that are difficult to detect. A previous study showed that antiplatelet therapy was not effective in slowing down the
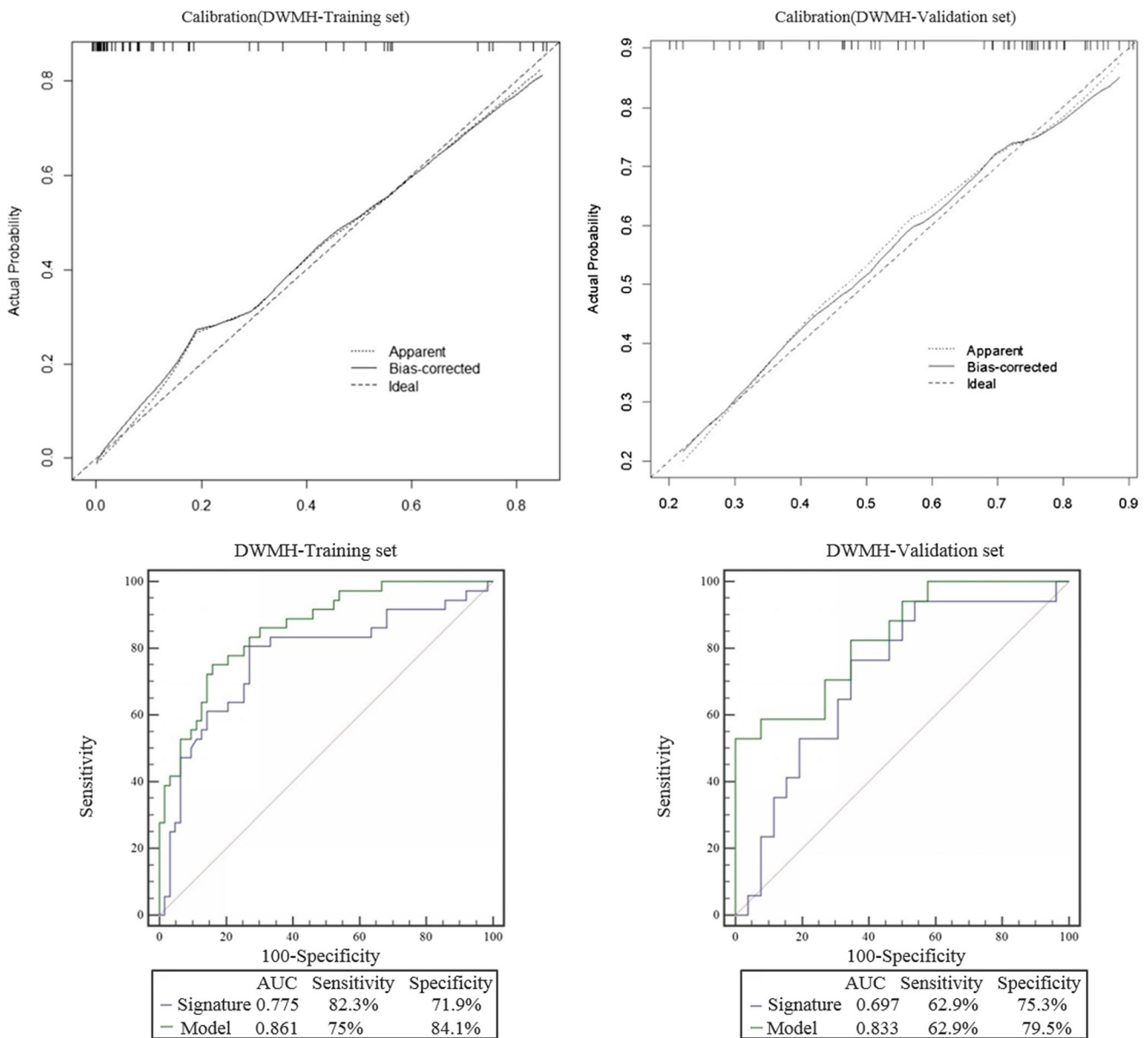
**Fig. 4** Calibration of the radiomics model for progression of DWMH in the training and validation sets. The dashed line represents a reference line where an ideal model would lie. The dotted line represents the performance of a hybrid model, while the solid line corrects for any bias in the hybrid model. The prediction performance of the ROC curves for AWMH and the AUC were 0.861 and 0.833, respectively

progression of WMH [28]. However, further studies are needed to determine if antihypertensive medications can decelerate the progression of WMH. Age was demonstrated as an independent risk factor for the progression of WMH, which is consistent with the literature [29, 30]. Interestingly, age was not found to be an independent risk factor for PWMH, which supports a previous pathological study showing that reduced vascular density in WMH was not associated with age [31]. Our research further demonstrated that only changes in PWMH were unrelated to age, which explains why the prediction model for PWMH showed the lowest performance. However, this conclusion

is limited, as this is a preliminary study using a small sample size. In addition, hyperlipidemia was shown to be a risk factor for the progression of WMH. Previous studies have shown that hyperlipidemia leads to microvascular hemodynamic regulation disorder [32, 33], which increases viscosity and resistance of blood flow [34]. We speculate that the PWMH burden is more likely to be determined by chronic hemodynamic effects (low perfusion). Hyperlipidemia may be related to other risk factors, such as high blood pressure or obesity, for the progression of WMH [35]. BMI was found to be an independent risk factor for the progression of DWMH, which is consistent
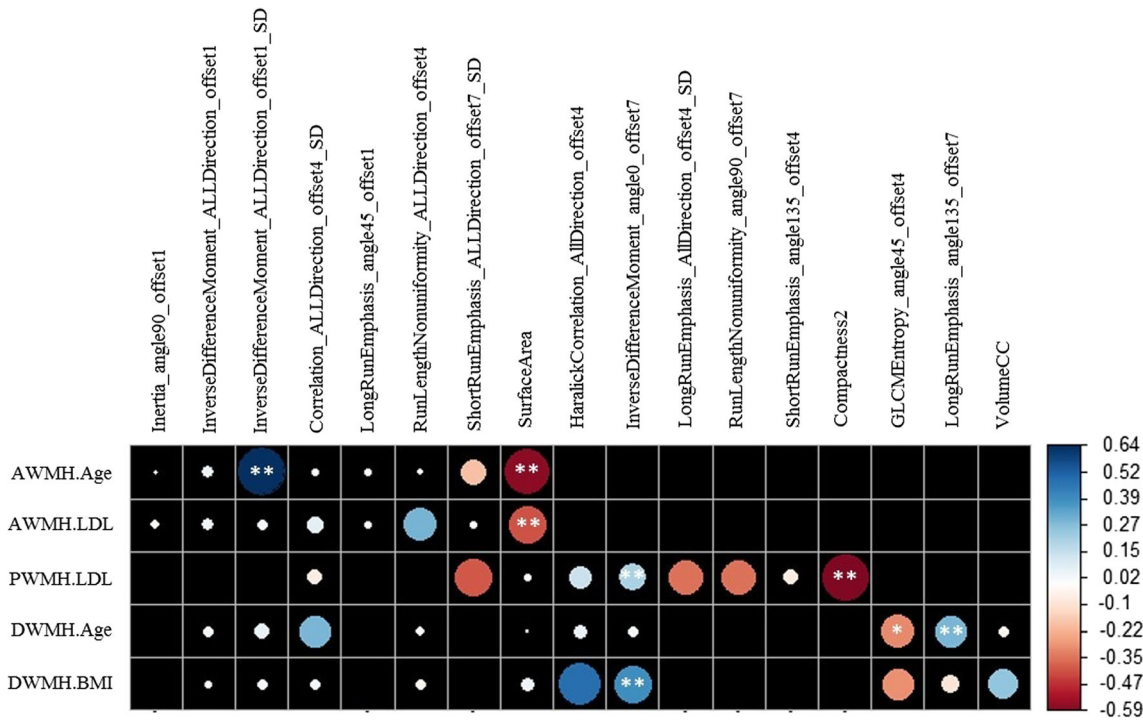
**Fig. 5** Correlation map between statistically significant clinical risk factors and features of the radiomics signature in each subgroup. The color bar on the right represents the size of the correlation coefficient; the larger the circle in the figure, the higher the correlation and vice versa. Asterisk indicates *p* < 0.05. Double asterisks indicate *p* < 0.005. AWMH, white matter hyperintensities in any (periventricular and/or deep) region; PWMH, periventricular white matter hyperintensities; DWMH, deep white matter hyperintensities; BMI, body mass index; LDL, low-density lipoprotein
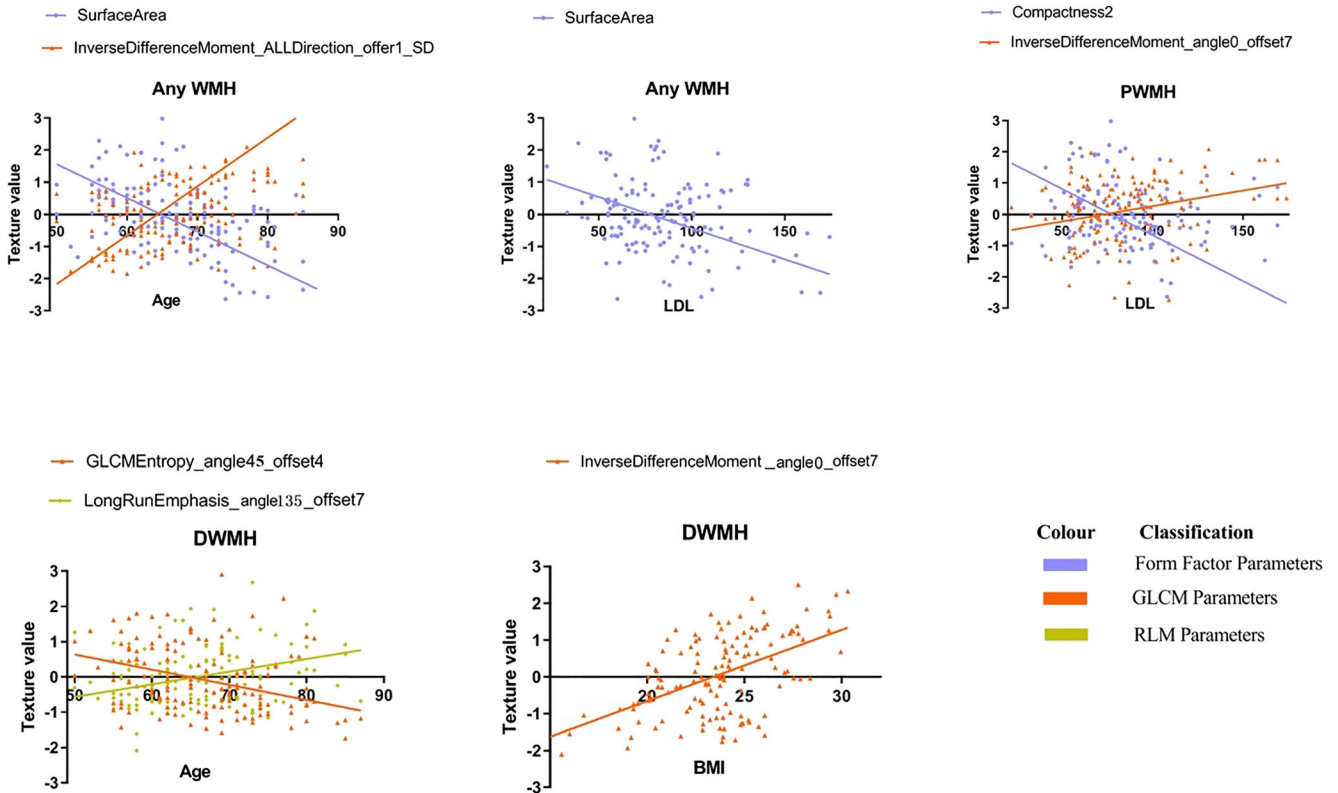


**Fig. 6** The scatter plots between the radiomics features and different independent risk factors. The different colors represent different feature categories

with the findings of Griffantia et al [36], indicating the progression of DWMH might be delayed by controlling the BMI of patients.

Many studies have investigated potential biomarkers for assessing the progression and severity of WMH [37, 38]. Compared with those biomarkers, radiomics may serve as a non-invasive biomarker to reflect white matter status. Our research showed that dimensionality-reduced features were primarily GLCM, RLM, and formfactor features, very similar to the existing study on the texture analysis of white matter [39, 40]; GLCM represents heterogeneity and homogeneity, which indirectly indicates the heterogeneity changes during the conversion from NAWM to WMH. The results are similar to a previous study by Loizou [41], who found that GLCM and formfactor features were significantly different in the progression of NAWM. Formfactor features, such as SurfaceArea, represent changes in volume, area, or shape that may reflect microscopic structures. The volume and morphology of WMH may change with age [40], which can also be confirmed by SurfaceArea being present in all three subgroups. In addition, the study showed that the RLM, which reflects roughness and directionality, was also associated with the progression of WMH, as features with directionality have a longer run length at a specific angle [42]. Healthy white matter fiber bundles are oriented and regulated, but myelin damaged causes them to lose their regular structure and become thickened and blurred [43], indicating that WMH progression could be indicated from WBWM using RLM, especially in the DMWH subgroup, which had a close correlation with age. This suggests that deep white matter is more susceptible to myelin damage over time, which is consistent with our results that the radiomics score was lowest in the DWMH subgroup. These results also indicate that the radiomics features of WBWM can reveal the relationship between the progression and risk factors of WMH in conventional MRI.

Our study has some limitations. First, we selected a single time interval for the progression of WMH, yet continuous changes cannot be fully observed in the process of NAWM converting to WMH. However, we could elucidate the pathological mechanism in the formation and progression of WMH based on radiomics features. Furthermore, we did not use volumetric measurements to assess the progression of WMH, which may lead to deviations in the assessment of progressive WMH. Nevertheless, the visual WMH changes scale used in the current study was highly correlated with changes in the volume of WMH [44]. Lastly, we performed a retrospective study in a single-center, and our results cannot be directly applied to patients at other institutions with WMH. Nevertheless, this study established a radiomics-based biomarker for assessing the progression of WMH using conventional MRI, which may be helpful in future multicenter prospective studies.

In conclusion, the radiomics analysis of WBWM showed that the progression of WMH involved diffuse damage far beyond visually hyperintense areas on conventional MRI sequences. High-risk populations with possible progressive WMH can be identified using radiomics of WBWM.

## Compliance with ethical standards

**Guarantor** The scientific guarantor of this publication is Zhenyu Shu.

**Conflict of interest** One of the authors of this manuscript (Peipei Pang) is an employee of GE Healthcare China. The remaining authors declare no relationships with any companies whose products or services may be related to the subject matter of the article.

**Statistics and biometry** One of the authors has significant statistical expertise.

**Informed consent** Written informed consent was waived by the Institutional Review Board.

**Ethical approval** Institutional Review Board approval was obtained.

**Study subjects or cohorts overlap** Some study subjects or cohorts have been previously reported in Shao Y, Chen Z, Ming S, et al Predicting the Development of Normal-Appearing White Matter With Radiomics in the Aging Brain: A Longitudinal Clinical Study. *Front Aging Neurosci* 2018;10:393.

**Methodology**
• Retrospective
• Diagnostic or prognostic study
• Performed at one institution

## References

1. Wardlaw JM, Smith C, Dichgans M (2013) Mechanisms of sporadic cerebral small vessel disease: insights from neuroimaging. Lancet Neurol 12:483–497
2. Maillard P, Fletcher E, Harvey D et al (2011) White matter hyperintensity penumbra. Stroke 42:1917–1922
3. Valdes Hernandez Mdel C, Armitage PA, Thrippleton MJ et al (2015) Rationale, design and methodology of the image analysis protocol for studies of patients with cerebral small vessel disease and mild stroke. Brain Behav 5:e00415
4. Taylor ANW, Kambeitz-Ilankovic L, Gesierich B et al (2017) Tract-specific white matter hyperintensities disrupt neural network function in Alzheimer's disease. Alzheimers Dement 13:225–235
5. Valdes Hernandez MDC, Gonzalez-Castro V, Chappell FM et al (2017) Application of texture analysis to study small vessel disease and blood-brain barrier integrity. Front Neurol 8:327
6. Lee WJ, Jung KH, Ryu YJ et al (2017) Progression of cerebral white matter hyperintensities and the associated sonographic index. Radiology 284:824–833

7. Holmegaard L, Jensen C, Redfors P, Blomstrand C, Jern C, Jood K (2018) Long-term progression of white matter hyperintensities in ischemic stroke. Acta Neurol Scand 138:548–556

8. Yip SS, Aerts HJ (2016) Applications and limitations of radiomics. Phys Med Biol 61:R150–R166

9. Liang C, Huang Y, He L et al (2016) The development and validation of a CT-based radiomics signature for the preoperative discrimination of stage I-II and stage III-IV colorectal cancer. Oncotarget 7: 31401–31412

10. Huang YQ, Liang CH, He L et al (2016) Development and validation of a radiomics nomogram for preoperative prediction of lymph node metastasis in colorectal cancer. J Clin Oncol 34:2157–2164

11. Abbasian Ardakani A, Gharbali A, Saniei Y, Mosarrezaii A, Nazarbaghi S (2015) Application of texture analysis in diagnosis of multiple sclerosis by magnetic resonance imaging. Glob J Health Sci 7:68–78

12. Holli KK, Harrison L, Dastidar P et al (2010) Texture analysis of MR images of patients with mild traumatic brain injury. BMC Med Imaging 10:8

13. Wardlaw JM, Valdes Hernandez MC, Munoz-Maniega S (2015) What are white matter hyperintensities made of? Relevance to vascular cognitive impairment. J Am Heart Assoc 4:001140

14. Promjunyakul N, Lahna D, Kaye JA et al (2015) Characterizing the white matter hyperintensity penumbra with cerebral blood flow measures. Neuroimage Clin 8:224–229

15. Shao Y, Chen Z, Ming S et al (2018) Predicting the development of normal-appearing white matter with radiomics in the aging brain: a longitudinal clinical study. Front Aging Neurosci 10:393

16. Prins ND, van Straaten EC, van Dijk EJ et al (2004) Measuring progression of cerebral white matter lesions on MRI: visual rating and volumetrics. Neurology 62:1533–1539

17. Kim KW, MacFall JR, Payne ME (2008) Classification of white matter lesions on magnetic resonance imaging in elderly persons. Biol Psychiatry 64:273–280

18. ten Dam VH, van den Heuvel DM, de Craen AJ et al (2007) Decline in total cerebral blood flow is linked with increase in periventricular but not deep white matter hyperintensities. Radiology 243:198–203

19. van den Heuvel DM, ten Dam VH, de Craen AJ et al (2006) Increase in periventricular white matter hyperintensities parallels decline in mental processing speed in a non-demented elderly population. J Neurol Neurosurg Psychiatry 77:149–153

20. Maillard P, Carmichael O, Fletcher E, Reed B, Mungas D, DeCarli C (2012) Coevolution of white matter hyperintensities and cognition in the elderly. Neurology 79:442–448

21. Park BY, Lee MJ, Lee SH et al (2018) DEWS (DEep White matter hyperintensity Segmentation framework): a fully automated pipeline for detecting small deep white matter hyperintensities in migraineurs. Neuroimage Clin 18:638–647

22. Fazekas F, Kleinert R, Offenbacher H et al (1993) Pathologic correlates of incidental MRI white matter signal hyperintensities. Neurology 43:1683–1689

23. Schmidt R, Schmidt H, Haybaeck J et al (2011) Heterogeneity in age-related white matter changes. Acta Neuropathol 122:171–185

24. Bernbaum M, Menon BK, Fick G et al (2015) Reduced blood flow in normal white matter predicts development of leukoaraiosis. J Cereb Blood Flow Metab 35:1610–1615

25. Nasel C, Boubela R, Kalcher K, Moser E (2017) Normalised time-to-peak-distribution curves correlate with cerebral white matter hyperintensities - could this improve early diagnosis? J Cereb Blood Flow Metab 37:444–455

26. Madden DJ, Spaniol J, Whiting WL et al (2007) Adult age differences in the functional neuroanatomy of visual attention: a combined fMRI and DTI study. Neurobiol Aging 28:459–476

27. Maillard P, Fletcher E, Lockhart SN et al (2014) White matter hyperintensities and their penumbra lie along a continuum of injury in the aging brain. Stroke 45:1721–1726

28. Yoon CW, Choi Y, Jeon S et al (2017) Is antiplatelet treatment effective at attenuating the progression of white matter hyperintensities? PLoS One 12:e0176300

29. Munoz Maniega S, Chappell FM, Valdes Hernandez MC et al (2017) Integrity of normal-appearing white matter: influence of age, visible lesion burden and hypertension in patients with small-vessel disease. J Cereb Blood Flow Metab 37:644–656

30. Grueter BE, Schulz UG (2012) Age-related cerebral white matter disease (leukoaraiosis): a review. Postgrad Med J 88:79–87

31. Moody DM, Thore CR, Anstrom JA, Challa VR, Langefeld CD, Brown WR (2004) Quantification of afferent vessels shows reduced brain vascular density in subjects with leukoaraiosis. Radiology 233:883–890

32. Stokes KY, Cooper D, Tailor A, Granger DN (2002) Hypercholesterolemia promotes inflammation and microvascular dysfunction: role of nitric oxide and superoxide. Free Radic Biol Med 33:1026–1036

33. VanTeeffelen JW, Constantinescu AA, Vink H, Spaan JA (2005) Hypercholesterolemia impairs reactive hyperemic vasodilation of 2A but not 3A arterioles in mouse cremaster muscle. Am J Physiol Heart Circ Physiol 289:H447–H454

34. Cho YI, Cho DJ, Rosenson RS (2014) Endothelial shear stress and blood viscosity in peripheral arterial disease. Curr Atheroscler Rep 16:404

35. Ryu WS, Woo SH, Schellingerhout D et al (2014) Grading and interpretation of white matter hyperintensities using statistical maps. Stroke 45:3567–3575

36. Griffanti L, Jenkinson M, Suri S et al (2018) Classification and characterization of periventricular and deep white matter hyperintensities on MRI: a study in older adults. Neuroimage 170:174–181

37. van Overbeek EC, Staals J, Knottnerus IL, ten Cate H, van Oostenbrugge RJ et al (2016) Plasma tPA-activity and progression of cerebral white matter hyperintensities in lacunar stroke patients. PLoS One 11:e0150740

38. Lee WJ, Jung KH, Ryu YJ et al (2017) Cystatin C, a potential marker for cerebral microvascular compliance, is associated with white-matter hyperintensities progression. PLoS One 12:e0184999

39. Harrison LC, Raunio M, Holli KK et al (2010) MRI texture analysis in multiple sclerosis: toward a clinical analysis protocol. Acad Radiol 17:696–707

40. Tozer DJ, Zeestraten E, Lawrence AJ, Barrick TR, Markus HS (2018) Texture analysis of T1-weighted and fluid-attenuated inversion recovery images detects abnormalities that correlate with cognitive decline in small vessel disease. Stroke 49:1656–1661

41. Loizou CP, Pattichis CS, Seimenis I et al (2009) Quantitative analysis of brain white matter lesions in multiple sclerosis subjects. International Conference on Information Technology & Applications in Biomedicine; 1–4

42. Li Z, Mao Y, Huang W et al (2017) Texture-based classification of different single liver lesion based on SPAIR T2W MRI images. BMC Med Imaging 17:42

43. Yu O, Steibel J, Mauss Y et al (2004) Remyelination assessment by MRI texture analysis in a cuprizone mouse model. Magn Reson Imaging 22:1139–1144

44. Gouw AA, van der Flier WM, van Straaten EC et al (2008) Reliability and sensitivity of visual scales versus volumetry for evaluating white matter hyperintensity progression. Cerebrovasc Dis 25:247–253